PERGAMON

International Journal of Solids and Structures 40 (2003) 7181–7196

INTERNATIONAL JOURNAL OF SOLIDS and STRUCTURES

www.elsevier.com/locate/ijsolstr

Three-dimensional analysis of transient thermal stresses in functionally graded plates

Senthil S. Vel [a,*], R.C. Batra [b]

[a] Department of Mechanical Engineering, University of Maine, 5711 Boardman Hall room 214, Orono, ME 04469-5711, USA
[b] Department of Engineering Science and Mechanics, M/C 0219, Virginia Polytechnic Institute and State University, Blacksburg, VA 24061, USA

Received 21 November 2002

Dedicated to George Dvorak for his pioneering contributions to Mechanics

Abstract

An analytical solution is presented for three-dimensional thermomechanical deformations of a simply supported functionally graded (FG) rectangular plate subjected to time-dependent thermal loads on its top and/or bottom surfaces. Material properties are taken to be analytical functions of the thickness coordinate. The uncoupled quasi-static linear thermoelasticity theory is adopted in which the change in temperature, if any, due to deformations is neglected. A temperature function that identically satisfies thermal boundary conditions at the edges and the Laplace transformation technique are used to reduce equations governing the transient heat conduction to an ordinary differential equation (ODE) in the thickness coordinate which is solved by the power series method. Next, the elasticity problem for the simply supported plate for each instantaneous temperature distribution is analyzed by using displacement functions that identically satisfy boundary conditions at the edges. The resulting coupled ODEs with variable coefficients are also solved by the power series method. The analytical solution is applicable to a plate of arbitrary thickness. Results are given for two-constituent metal-ceramic FG rectangular plates with a power-law through-the-thickness variation of the volume fraction of the constituents. The effective elastic moduli at a point are determined by either the Mori–Tanaka or the self-consistent scheme. The transient temperature, displacements, and thermal stresses at several critical locations are presented for plates subjected to either time-dependent temperature or heat flux prescribed on the top surface. Results are also given for various volume fractions of the two constituents, volume fraction profiles and the two homogenization schemes.

Keywords: Rectangular plate; Simply supported edges; Thermomechanical deformations; Laplace transform

1. Introduction

Laminated composite plates are extensively used due to their high specific strength and high specific stiffness. However, the abrupt change in material properties across an interface between discrete materials introduces large interlaminar stresses that could cause delamination. One way to overcome this adverse effect

* Corresponding author. Tel.: +1-207-581-2777; fax: +1-207-581-2379.
E-mail address: vel@umeme.maine.edu (S.S. Vel).

doi:10.1016/S0020-7683(03)00361-5

is to use functionally graded materials (FGMs). In a functionally graded (FG) plate, the volume fraction of the constituent materials changes gradually, usually in the thickness direction only. A smooth variation of in-plane material properties and an optimum response to external thermomechanical loads could also be obtained by changing gradually the chemical structure of a thin polymer sheet (Lambros et al., 1999; Breval et al., 1990). Recently Vel and Batra (2003a, 2002) presented a three-dimensional (3D) exact solution for the mechanical vibrations and the steady state thermal stresses in a simply supported FG rectangular plate. Vel and Batra (2003b) have also given an exact solution for static thermoelastic cylindrical bending deformations of an FG plate. Since the magnitudes of transient thermal stresses are usually larger than those of steady state stresses, it is important to quantify them for proper design of an FG plate. Many of the earlier studies on thermal stresses in FG plates are based on plate theories. For example, Yang and Shen (2002) have presented a free and forced vibration analysis of initially stressed FG plates in a thermal environment based on a higher order shear deformation plate theory. Cheng and Batra (2000) have used the asymptotic expansion method to study the 3D thermoelastic deformations of an FG elliptic plate. Tarn and Wang (1995) have also given an asymptotic solution for nonhomogeneous plates. Reiter et al. (1997) and Reiter and Dvorak (1997, 1998) conducted detailed finite element studies of discrete models containing simulated skeletal and particulate microstructures and compared results with those computed from homogenized models in which effective properties were derived by either the Mori–Tanaka or the self-consistent methods.

Some attempts have been made to analyze the 3D transient temperature distribution and thermal stresses in FG plates. For example, Ootao and Tanigawa (1999) have approximated an FG plate as a laminated plate consisting of a series of laminae, with each lamina assigned slightly different material properties. Kim and Noda (2001) adopted a laminate theory and obtained Green's function solution for analysing the 3D transient temperature distribution.

Jin and Batra (1996a,b, 1998), amongst others, have used the quasi-static 2D linear thermoelasticity theory to study fracture characteristics at a crack tip in an FG plate. They found that the fracture toughness is significantly increased when a crack grows from the ceramic-rich region into the metal-rich region in an aluminum–nickel FGM. Here we present an analytical solution for the 3D transient thermal stresses of an FG thick plate. We assume that the macroscopic properties of the plate material are isotropic and vary smoothly in the thickness direction. We expand material properties as a Taylor series in the thickness direction thus circumventing the laminate theory approximation. A temperature function that identically satisfies thermal boundary conditions at the edges and the Laplace transformation technique are employed to reduce equations governing the transient heat conduction to an ordinary differential equation (ODE) in the thickness coordinate, which is then solved by the power series method. The uncoupled quasi-static linear thermoelasticity theory is adopted in which changes in temperature, if any, due to deformations are neglected. Displacement functions that identically satisfy mechanical boundary conditions at the edges are used to reduce the partial differential equations governing the mechanical deformations to a set of coupled ODEs in the thickness coordinate, which are solved by the power series method.

We consider an Al/SiC graded plate with a power-law variation of the volume fractions of the constituents through the thickness. The effective elastic moduli at a point are determined from the local volume fractions of the constituents and their material properties either by the Mori and Tanaka (1973) or the self-consistent (Hill, 1965) scheme. The temperature, displacements, and stresses at critical locations for transient thermal loads are given for the two homogenization schemes, volume fractions of the constituents, and the exponent in the power-law that gives through-the-thickness variation of the constituents.

2. Formulation of the problem

Fig. 1 shows a sketch of the problem studied. We use rectangular Cartesian coordinates x_i $(i = 1, 2, 3)$ to describe the thermomechanical fields in a plate occupying the region $[0, L_1] \times [0, L_2] \times [-H/2, H/2]$ in the

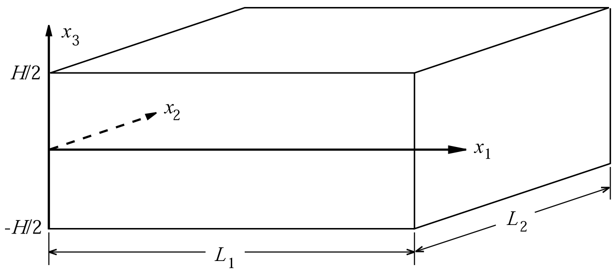

Fig. 1. The FG rectangular plate and the coordinate system.

unstressed reference configuration at a uniform temperature. The plate is made of an isotropic material with material properties varying smoothly in the x_3 (thickness) direction only.

The analysis is based on the uncoupled, quasi-static linear thermoelasticity theory wherein both, the change in temperature of the elastic body due to working of elastic deformations, and the inertia term in the equations of motion, are neglected (e.g. see Fung and Tong, 2001). In a consistent linear thermoelasticity theory for a body unstressed in the reference configuration, the elastic working is a second-order effect and is hence ignored. Thus the heat equation in the absence of internal heat sources and the equations of motion in the absence of body forces reduce to

$$c\rho\dot{T} = -q_{j,j}, \quad \sigma_{ij,j} = 0 \qquad (i,j = 1,2,3), \tag{1}$$

where c, ρ, T, q_j and σ_{ij} are the specific heat capacity, mass density, change in temperature of a material particle from that in the stress-free reference configuration, the heat flux and the Cauchy stress tensor, respectively. A comma followed by index j denotes partial differentiation with respect to the position x_j of a material particle, a superimposed dot indicates partial derivative with respect to time t, and a repeated index implies summation over the range of the index.

The constitutive equations for a linear isotropic thermoelastic material are (e.g. see Fung and Tong, 2001)

$$\begin{aligned} \sigma_{ij} &= \lambda\varepsilon_{kk}\delta_{ij} + 2\mu\varepsilon_{ij} - \beta\delta_{ij}T, \\ q_j &= -\kappa T_{,j}, \end{aligned} \tag{2}$$

where λ and μ are the Lamé constants, β is the stress–temperature modulus, κ is the thermal conductivity, ε_{ij} is the infinitesimal strain tensor and δ_{ij} is the Kronecker delta. The material properties c, ρ, λ, μ, β and κ are functions of x_3.

The infinitesimal strain tensor is related to the mechanical displacements u_i by

$$\varepsilon_{ij} = \tfrac{1}{2}(u_{i,j} + u_{j,i}). \tag{3}$$

The edges of the plate are assumed to be simply supported and maintained at the reference temperature. That is,

$$\begin{aligned} &\sigma_{11} = 0, \quad u_2 = u_3 = 0, \quad T = 0 \quad \text{at } x_1 = 0, L_1, \\ &\sigma_{22} = 0, \quad u_1 = u_3 = 0, \quad T = 0 \quad \text{at } x_2 = 0, L_2. \end{aligned} \tag{4}$$

The thermal boundary conditions on the top and the bottom surfaces are specified as

$$\vartheta^{\pm}T(x_1,x_2,\pm H/2,t) + \xi^{\pm}q_3(x_1,x_2,\pm H/2,t) = \varphi^{\pm}(t)\sin ax_1 \sin bx_2, \tag{5}$$

where $\varphi^+(t)$ and $\varphi^-(t)$ are known functions, $a = k\pi/L_1$, $b = m\pi/L_2$, and k and m are positive integers. By appropriately choosing values of constants $\vartheta^{\pm}$ and $\xi^{\pm}$, various boundary conditions corresponding to either a prescribed temperature, a prescribed heat flux or exposure to an ambient temperature through a boundary conductance can be specified on the top and bottom surfaces of the plate. Any prescribed temperature distribution or heat flux on the top surface can be expressed in terms of a double Fourier series and the solution obtained by the method of superposition. The mechanical boundary conditions prescribed on the top and the bottom surfaces can be either a displacement component u_j or a traction component σ_{3j}. Since we are interested in the transient thermal stresses, the top and bottom surfaces are taken to be traction free. That is,

$$\sigma_{13} = \sigma_{23} = \sigma_{33} = 0 \quad \text{at } x_3 = \pm H/2. \tag{6}$$

Since T equals the change in temperature, therefore, $T(x_1, x_2, x_3, 0) = 0$. The mechanical and the thermal problems are one-way coupled in the sense that the temperature field is determined first by solving Eqs. $(1)_1$ and $(2)_2$ and the pertinent boundary and initial conditions, and the displacements are obtained for each instantaneous temperature distribution from Eqs. $(1)_2$ and $(2)_1$ and the relevant boundary conditions.

3. A three-dimensional analytical solution

We assume that the material properties are analytic functions of x_3 and thus can be represented by a Taylor series expansion about the midsurface as

$$[\lambda, \mu, \beta, \kappa, c\rho] = \sum_{\alpha=0}^{\infty} \left[\tilde{\lambda}^{(\alpha)}, \tilde{\mu}^{(\alpha)}, \tilde{\beta}^{(\alpha)}, \tilde{\kappa}^{(\alpha)}, \tilde{\zeta}^{(\alpha)}\right] x_3^{\alpha}. \tag{7}$$

Since λ, μ, β, κ and $c\rho$ have positive values for all x_3, therefore $\tilde{\lambda}^{(0)}$, $\tilde{\mu}^{(0)}$, $\tilde{\beta}^{(0)}$, $\tilde{\kappa}^{(0)}$ and $\tilde{\zeta}^{(0)}$ are positive.

3.1. The heat conduction problem

A solution for the change in temperature is sought in the form

$$T(x_1, x_2, x_3, t) = \theta(x_3, t) \sin ax_1 \sin bx_2, \tag{8}$$

which identically satisfies boundary conditions $(4)_{4,8}$ at the edges of the plate. We will require that $\theta(x_3, 0) = 0$. Substitution for T from (8) into $(2)_2$ and the result into $(1)_1$ gives the following partial differential equation with variable coefficients,

$$\kappa[(a^2 + b^2)\theta - \theta''] - \kappa'\theta' + c\rho\dot{\theta} = 0, \tag{9}$$

where a prime denotes derivative with respect to x_3. Taking the Laplace Transform $\mathscr{L}$ of (9) with respect to time t and defining $\Theta(x_3, s) \equiv \mathscr{L}[\theta(x_3, t)]$, we obtain the following ODE involving only spatial derivatives of Θ

$$\kappa[(a^2 + b^2)\Theta - \Theta''] - \kappa'\Theta' + c\rho s\Theta = 0. \tag{10}$$

We assume a solution for Θ in the form of a power series

$$\Theta(x_3, s) = \sum_{\gamma=0}^{\infty} \tilde{\Theta}^{(\gamma)}(s) x_3^{\gamma}. \tag{11}$$

The series (11) and the Taylor series for κ and $c\rho$ in (7) are substituted into Eq. (10). By multiplying the infinite series, appropriately shifting the index of summation and equating each power of x_3 to zero, we obtain the recursive relation

$$\sum_{\gamma=0}^{\alpha} \tilde{\kappa}^{(\gamma)}[\tilde{\Theta}^{(\alpha-\gamma+2)}(\alpha-\gamma+2)(\alpha-\gamma+1) - \tilde{\Theta}^{(\alpha-\gamma)}(a^2+b^2)] + \tilde{\kappa}^{(\gamma+1)}\tilde{\Theta}^{(\alpha-\gamma+1)}(\gamma+1)(\alpha-\gamma+1)$$
$$- s\tilde{\zeta}^{(\gamma)}\tilde{\Theta}^{(\alpha-\gamma)} = 0, \tag{12}$$

for $\alpha = 0, 1, 2, \ldots$ Since $\tilde{\kappa}^{(0)} > 0$, corresponding to $\alpha = 0$ in (12) we obtain

$$\tilde{\Theta}^{(2)}(s) = \frac{1}{2}\left[(a^2+b^2) + s\frac{\tilde{\zeta}^{(0)}}{\tilde{\kappa}^{(0)}}\right]\tilde{\Theta}^{(0)}(s) - \frac{\tilde{\kappa}^{(1)}}{2\tilde{\kappa}^{(0)}}\tilde{\Theta}^{(1)}(s). \tag{13}$$

Evaluation of the recursion formula (12) successively for $\alpha = 1, 2, \ldots$, gives $\tilde{\Theta}^{(\alpha+2)}(s)$ in terms of arbitrary functions $\tilde{\Theta}^{(0)}(s)$ and $\tilde{\Theta}^{(1)}(s)$. Substitution of the coefficients $\tilde{\Theta}^{(\alpha)}(s)$ into (11) gives

$$\Theta(x_3, s) = \tilde{\Theta}^{(0)}(s)\psi_0(x_3, s) + \tilde{\Theta}^{(1)}(s)\psi_1(x_3, s), \tag{14}$$

where $\psi_0(x_3, s)$ and $\psi_1(x_3, s)$ are known infinite series in x_3 whose coefficients are polynomials in s, and $\tilde{\Theta}^{(0)}(s)$ and $\tilde{\Theta}^{(1)}(s)$ are unknown functions that are determined by satisfying the boundary conditions on the top and bottom surfaces.

Using (8) and $(2)_2$, the thermal boundary conditions (5) on the top and bottom surfaces are

$$\vartheta^{\pm}\theta(\pm H/2, t) - \xi^{\pm}\kappa(\pm H/2)\theta'(\pm H/2, t) = \varphi^{\pm}(t). \tag{15}$$

Taking the Laplace transform of (15) with respect to t, we obtain

$$\vartheta^{\pm}\Theta(\pm H/2, s) - \xi^{\pm}\kappa(\pm H/2)\Theta'(\pm H/2, s) = \Phi^{\pm}(s), \tag{16}$$

where $\Phi^{\pm}(s) \equiv \mathscr{L}[\varphi^{\pm}(t)]$. Substitution of (14) into (16) gives

$$\vartheta^{\pm}[\tilde{\Theta}^{(0)}(s)\psi_0(\pm H/2, s) + \tilde{\Theta}^{(1)}(s)\psi_1(\pm H/2, s)] - \xi^{\pm}\kappa(\pm H/2)[\tilde{\Theta}^{(0)}(s)\psi_0'(\pm H/2, s) + \tilde{\Theta}^{(1)}(s)\psi_1'(\pm H/2, s)]$$
$$= \Phi^{\pm}(s). \tag{17}$$

This equation is readily solved to obtain the following expressions for $\tilde{\Theta}^{(0)}(s)$ and $\tilde{\Theta}^{(1)}(s)$

$$\begin{aligned}
\tilde{\Theta}^{(0)}(s) &= \frac{1}{D}\Big\{[\vartheta^{-}\psi_1(-H/2, s) - \xi^{-}\kappa(-H/2)\psi_1'(-H/2, s)]\Phi^{+}(s) \\
&\qquad - [\vartheta^{+}\psi_1(H/2, s) - \xi^{+}\kappa(H/2)\psi_1'(H/2, s)]\Phi^{-}(s)\Big\}, \\
\tilde{\Theta}^{(1)}(s) &= \frac{1}{D}\Big\{[\vartheta^{+}\psi_0(H/2, s) - \xi^{+}\kappa(H/2)\psi_0'(H/2, s)]\Phi^{-}(s) \\
&\qquad - [\vartheta^{-}\psi_0(-H/2, s) - \xi^{-}\kappa(-H/2)\psi_0'(-H/2, s)]\Phi^{+}(s)\Big\},
\end{aligned} \tag{18}$$

where

$$\begin{aligned}
D = {} & [\vartheta^{+}\psi_0(H/2, s) - \xi^{+}\kappa(H/2)\psi_0'(H/2, s)][\vartheta^{-}\psi_1(-H/2, s) - \xi^{-}\kappa(-H/2)\psi_1'(-H/2, s)] \\
& - [\vartheta^{-}\psi_0(-H/2, s) - \xi^{-}\kappa(-H/2)\psi_0'(-H/2, s)][\vartheta^{+}\psi_1(H/2, s) - \xi^{+}\kappa(H/2)\psi_1'(H/2, s)].
\end{aligned} \tag{19}$$

Substitution of (18) into (14) gives the function $\Theta(x_3, s)$ in the form of a power series in x_3, whose coefficients are rational functions of s. By writing these coefficients as partial fractions of s and taking the inverse Laplace transform, we obtain

$$\theta(x_3, t) = \sum_{\gamma=0}^{\infty} \tilde{\theta}^{(\gamma)}(t)x_3^{\gamma}, \tag{20}$$

and the transient temperature field $T(x_1, x_2, x_3, t)$ for the plate is determined from (8).

3.2. The displacement field and thermal stresses

A solution for the displacement field is sought in the form

$$\begin{aligned} u_1 &= U_1(x_3)\cos ax_1 \sin bx_2, \\ u_2 &= U_2(x_3)\sin ax_1 \cos bx_2, \\ u_3 &= U_3(x_3)\sin ax_1 \sin bx_2, \end{aligned} \tag{21}$$

which identically satisfies the homogeneous boundary conditions $(4)_{1-3}$ and $(4)_{5-7}$ at the simply supported edges. Substitution for $\mathbf{u}$ from (21) into (3), for ε and T into (2) and for $\boldsymbol{\sigma}$ into $(1)_2$ gives the following coupled system of second-order ODEs:

$$\begin{aligned} &(\lambda+2\mu)U_1a^2+\lambda U_2ab+\mu(U_1b^2+U_2ab)-\lambda U_3'a-\mu'(U_1'+U_3a)-\mu(U_1''+U_3'a)+\beta\theta a=0, \\ &(\lambda+2\mu)U_2b^2+\lambda U_1ab+\mu(U_2b^2+U_1ab)-\lambda U_3'b-\mu'(U_2'+U_3b)-\mu(U_2''+U_3'b)+\beta\theta b=0, \\ &\mu(U_1'a+U_2'b)+\mu U_3(a^2+b^2)+\lambda'(U_1a+U_2b)+\lambda(U_1'a+U_2'b)-(\lambda'+2\mu')U_3' \\ &\quad -(\lambda+2\mu)U_3''+\beta'\theta+\beta\theta'=0. \end{aligned} \tag{22}$$

We assume a power series solution for the displacements as

$$U_i(x_3)=\sum_{\gamma=0}^{\infty}\widetilde{U}_i^{(\gamma)}x_3^{\gamma}. \tag{23}$$

Inserting into the ODEs (22) the material properties λ, μ and β from (7) and the assumed power series solution for the displacements and the temperature change from (23) and (20), we obtain the following coupled recurrence algebraic relations for every non-negative integer α:

$$\begin{aligned} &\sum_{\gamma=0}^{\alpha}(\tilde{\lambda}^{(\gamma)}+2\tilde{\mu}^{(\gamma)})\widetilde{U}_1^{(\alpha-\gamma)}a^2+\tilde{\lambda}^{(\gamma)}\widetilde{U}_2^{(\alpha-\gamma)}ab+\tilde{\mu}^{(\gamma)}(\widetilde{U}_1^{(\alpha-\gamma)}b^2+\widetilde{U}_2^{(\alpha-\gamma)}ab)-(\alpha-\gamma+1)\tilde{\lambda}^{(\gamma)}\widetilde{U}_3^{(\alpha-\gamma+1)}a \\ &\quad -(\gamma+1)\tilde{\mu}^{(\gamma+1)}((\alpha-\gamma+1)\widetilde{U}_1^{(\alpha-\gamma+1)}+\widetilde{U}_3^{(\alpha-\gamma)}a)-(\alpha-\gamma+1)\tilde{\mu}^{(\gamma)}((\alpha-\gamma+2)\widetilde{U}_1^{(\alpha-\gamma+2)} \\ &\quad +\widetilde{U}_3^{(\alpha-\gamma+1)}a)+\tilde{\beta}^{(\gamma)}\tilde{\theta}^{(\alpha-\gamma)}(t)a=0, \\ &\sum_{\gamma=0}^{\alpha}(\tilde{\lambda}^{(\gamma)}+2\tilde{\mu}^{(\gamma)})\widetilde{U}_2^{(\alpha-\gamma)}b^2+\tilde{\lambda}^{(\gamma)}\widetilde{U}_1^{(\alpha-\gamma)}ab+\tilde{\mu}^{(\gamma)}(\widetilde{U}_2^{(\alpha-\gamma)}a^2+\widetilde{U}_1^{(\alpha-\gamma)}ab)-(\alpha-\gamma+1)\tilde{\lambda}^{(\gamma)}\widetilde{U}_3^{(\alpha-\gamma+1)}b \\ &\quad -(\gamma+1)\tilde{\mu}^{(\gamma+1)}((\alpha-\gamma+1)\widetilde{U}_2^{(\alpha-\gamma+1)}+\widetilde{U}_3^{(\alpha-\gamma)}b)-(\alpha-\gamma+1)\tilde{\mu}^{(\gamma)}((\alpha-\gamma+2)\widetilde{U}_2^{(\alpha-\gamma+2)} \\ &\quad +\widetilde{U}_3^{(\alpha-\gamma+1)}b)+\tilde{\beta}^{(\gamma)}\tilde{\theta}^{(\alpha-\gamma)}(t)b=0, \\ &\sum_{\gamma=0}^{\alpha}\tilde{\mu}^{(\gamma)}(\alpha-\gamma+1)(\widetilde{U}_1^{(\alpha-\gamma+1)}a+\widetilde{U}_2^{(\alpha-\gamma+1)}b)+\tilde{\mu}^{(\gamma)}\widetilde{U}_3^{(\alpha-\gamma)}(a^2+b^2)+(\gamma+1)\tilde{\lambda}^{(\gamma+1)}(\widetilde{U}_1^{(\alpha-\gamma)}a+\widetilde{U}_2^{(\alpha-\gamma)}b) \\ &\quad +(\alpha-\gamma+1)\tilde{\lambda}^{(\gamma)}(\widetilde{U}_1^{(\alpha-\gamma+1)}a+\widetilde{U}_2^{(\alpha-\gamma+1)}b)-(\gamma+1)(\alpha-\gamma+1)(\tilde{\lambda}^{(\gamma+1)}+2\tilde{\mu}^{(\gamma+1)})\widetilde{U}_3^{(\alpha-\gamma+1)} \\ &\quad -(\alpha-\gamma+2)(\alpha-\gamma+1)(\tilde{\lambda}^{(\gamma)}+2\tilde{\mu}^{(\gamma)})\widetilde{U}_3^{(\alpha-\gamma+2)}-\tilde{\beta}^{(\gamma+1)}(\gamma+1)\tilde{\theta}^{(\alpha-\gamma)}(t) \\ &\quad -\tilde{\beta}^{(\gamma)}(\alpha-\gamma+1)\tilde{\theta}^{(\alpha-\gamma+1)}(t)=0. \end{aligned} \tag{24}$$

The recurrence relations (24) are evaluated successively for $\alpha = 0, 1, \ldots,$ to obtain $\widetilde{U}_1^{(\alpha+2)}$, $\widetilde{U}_2^{(\alpha+2)}$ and $\widetilde{U}_3^{(\alpha+2)}$ in terms of six arbitrary constants $\widetilde{U}_1^{(0)}$, $\widetilde{U}_1^{(1)}$, $\widetilde{U}_2^{(0)}$, $\widetilde{U}_2^{(1)}$, $\widetilde{U}_3^{(0)}$ and $\widetilde{U}_3^{(1)}$. These six constants are determined by satisfying the mechanical boundary conditions (6) on the top and the bottom surfaces of the plate. Thus displacements and stresses at any point in the entire plate can be determined.

4. Effective moduli of two-phase composites

Consider a FG composite material fabricated by mixing two distinct material phases, for example, a metal and a ceramic. Often, precise information about the size, shape and distribution of the particles is not available and the effective moduli of the graded composite must be evaluated based only on the volume fraction distributions and the approximate shape of the dispersed phase. Several micromechanics models have been developed to infer the effective properties of an equivalent macroscopically homogeneous composite material. We use here the Mori–Tanaka and the self-consistent methods to determine the effective moduli.

4.1. The Mori–Tanaka estimate

The Mori–Tanaka (Mori and Tanaka, 1973; Reiter and Dvorak, 1997) scheme for estimating the effective moduli is applicable to regions of the graded microstructure which have a well-defined continuous matrix and a randomly distributed particulate phase. It takes into account the interaction of the elastic fields among neighboring inclusions. It is assumed that the matrix phase, denoted by the subscript 1, is reinforced by spherical particulates, denoted by the subscript 2. In this notation, K_1, μ_1, κ_1 and α_1 denote the bulk modulus, the shear modulus, the thermal conductivity and the thermal expansion coefficient, respectively, and V_1 the volume fraction of the matrix phase. K_2, μ_2, κ_2, α_2 and V_2 denote the corresponding quantities for the particulate phase. It should be noted that $V_1 + V_2 = 1$, the Lamé constant λ is related to the bulk and the shear moduli by $\lambda = K - 2\mu/3$ and the stress–temperature modulus is related to the coefficient of thermal expansion by $\beta = (3\lambda + 2\mu)\alpha = 3K\alpha$. The effective value of $c\rho$ at a point in the composite is given by the "rule of mixture":

$$c\rho = c_1\rho_1 V_1 + c_2\rho_2 V_2. \tag{25}$$

For an isotropic matrix containing isotropic particulates, the macroscopic response of the composite is assumed to be isotropic. The effective local bulk modulus K and the effective shear modulus μ are given by

$$\begin{aligned} \frac{K - K_1}{K_2 - K_1} &= V_2 \Big/ \left(1 + (1 - V_2)\frac{K_2 - K_1}{K_1 + (4/3)\mu_1}\right), \\ \frac{\mu - \mu_1}{\mu_2 - \mu_1} &= V_2 \Big/ \left(1 + (1 - V_2)\frac{\mu_2 - \mu_1}{\mu_1 + f_1}\right), \end{aligned} \tag{26}$$

where $f_1 = \mu_1(9K_1 + 8\mu_1)/6(K_1 + 2\mu_1)$. The effective thermal conductivity κ is found from (Hatta and Taya, 1985)

$$\frac{\kappa - \kappa_1}{\kappa_2 - \kappa_1} = \frac{V_2}{1 + (1 - V_2)(\kappa_2 - \kappa_1)/3\kappa_1}, \tag{27}$$

and the coefficient of thermal expansion α is determined from the correspondence relation (Rosen and Hashin, 1970)

$$\frac{\alpha - \alpha_1}{\alpha_2 - \alpha_1} = \left(\frac{1}{K} - \frac{1}{K_1}\right) \Big/ \left(\frac{1}{K_2} - \frac{1}{K_1}\right). \tag{28}$$

4.2. Self-consistent estimate

The self-consistent method (Hill, 1965; Reiter and Dvorak, 1997) assumes that an inclusion is embedded in a continuum material whose effective properties are those of the composite. This method treats the matrix and reinforcement phases symmetrically and the same overall moduli is predicted for another composite in which the roles of the two phases are interchanged. This makes it particularly suitable for determining the effective moduli in those regions which have an interconnected skeletal microstructure. The effective moduli are given implicitly by

$$\begin{aligned} \delta/K &= V_1/(K-K_2) + V_2/(K-K_1), \\ \eta/\mu &= V_1/(\mu-\mu_2) + V_2/(\mu-\mu_1), \end{aligned} \tag{29}$$

where $\delta = 3 - 5\eta = K/(K + 4\mu/3)$. Eq. $(29)_1$ is solved for K in terms of μ to obtain

$$K = 1/(V_1/(K_1 + 4\mu/3) + V_2/(K_2 + 4\mu/3)) - 4\mu/3, \tag{30}$$

and μ is obtained by solving the following quadratic equation

$$[V_1K_1/(K_1 + 4\mu/3) + V_2K_2/(K_2 + 4\mu/3)] + 5[V_1\mu_2/(\mu-\mu_2) + V_2\mu_1/(\mu-\mu_1)] + 2 = 0. \tag{31}$$

The thermal conductivity (Hashin, 1968) is also given implicitly by

$$V_1(\kappa_1 - \kappa)/(\kappa_1 + 2\kappa) + V_2(\kappa_2 - \kappa)/(\kappa_2 + 2\kappa) = 0. \tag{32}$$

The coefficient of thermal expansion α is obtained by substitution for the self-consistent estimate of the bulk modulus K from (30) into the correspondence relation (28). Because the quadratic Eq. (31) and the quadratic Eq. (32) have to be solved to obtain the shear modulus μ and the thermal conductivity κ, it is easier to use the Mori–Tanaka method than the self-consistent scheme.

5. Results and discussion

We present exact results for a simply supported square plate with its top surface subjected to a transient thermal load. Since it is common in high-temperature applications to employ a ceramic top layer as a thermal barrier to a metallic structure, we choose the constituent materials of the FG plate to be Aluminum and SiC having the following material properties

$$\begin{aligned} \text{Al}: \quad & E_m = 70\ \text{GPa}, \quad \nu_m = 0.3, \quad \alpha_m = 23.4 \times 10^{-6}/\text{K}, \\ & \kappa_m = 233\ \text{W/mK}, \quad c_m = 896\ \text{J/kg K}, \quad \rho_m = 2707\ \text{kg/m}^3, \\ \text{SiC}: \quad & E_c = 427\ \text{GPa}, \quad \nu_c = 0.17, \quad \alpha_c = 4.3 \times 10^{-6}/\text{K}, \\ & \kappa_c = 65\ \text{W/mK}, \quad c_c = 670\ \text{J/kg K}, \quad \rho_c = 3100\ \text{kg/m}^3. \end{aligned} \tag{33}$$

We assume that the volume fraction of the ceramic phase is given by the power-law type function

$$V_c = V_c^- + (V_c^+ - V_c^-)\left(\frac{1}{2} + \frac{x_3}{H}\right)^p. \tag{34}$$

Here V_c^+ and V_c^- are, respectively, the volume fractions of the ceramic phase on the top and the bottom surfaces of the plate, and the parameter p dictates the volume fraction profile through the thickness. The dimensions of the simply supported plate are $L_1 = L_2 = 0.25$ m. For $V_c^- = 0$ and $V_c^+ = 1$ and different values of p, we have plotted in Fig. 2 the through-the-thickness variations of various material parameters given by the two homogenization schemes.

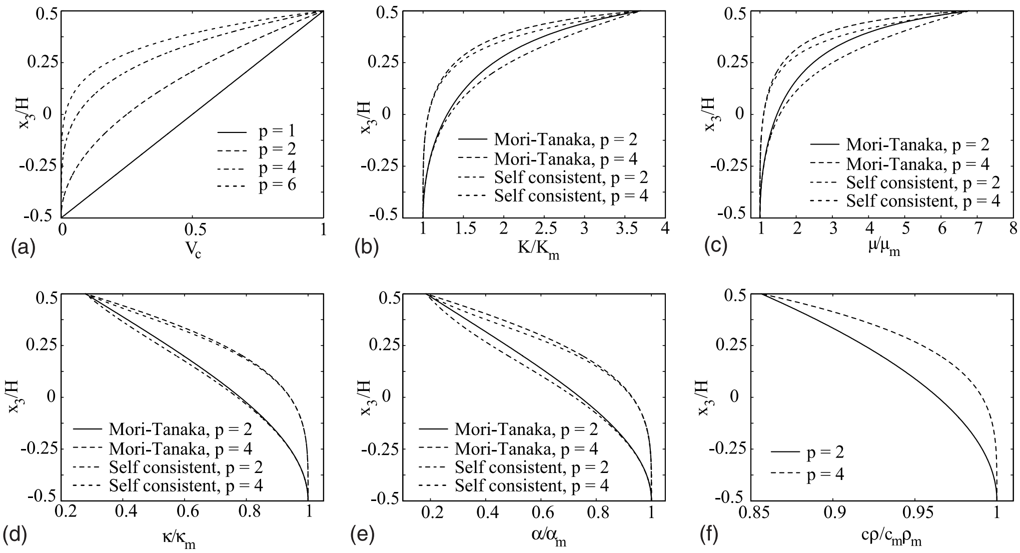

Fig. 2. Through-the-thickness variation of (a) ceramic volume fraction (b) bulk modulus (c) shear modulus, (d) thermal conductivity, (e) thermal expansion coefficient, and (f) specific heat capacity using the Mori–Tanaka and self-consistent homogenization schemes for different values of the power-law exponent p; $V_c^- = 0$, $V_c^+ = 1$.

A convergence study for the number of terms to be included in series (11) was performed for the temperature and heat flux prescribed on the top surface of the plate; the results for the latter case are summarized in Table 1. It is clear that 15 terms in the series (11) give accurate temperature fields in the plate. Obtaining the inverse Laplace Transform becomes more involved as we increase the number of terms in the series. The stresses and displacements were obtained by retaining 100 terms in the series expansion (23).

5.1. Time-dependent surface temperature

We first study the problem when the prescribed temperature on the top surface of the plate increases exponentially from the reference temperature to a prescribed steady state value given by

$$T(x_1, x_2, H/2, t) = T^+(1 - e^{-\gamma t}) \sin(\pi x_1/L_1) \sin(\pi x_2/L_2). \tag{35}$$

The bottom surface is maintained at the reference temperature, i.e., $T(x_1, x_2, -H/2, t) = 0$. The parameter γ determines the rate of temperature change on the top surface. Results are presented in terms of the non-dimensional variables defined as

Table 1
Computed temperature at three points in the plate for the heat flux (37) prescribed on the top surface of the plate with the bottom surface thermally insulated; $L/H = 5$ and non-dimensional variables are defined in Eq. (38)

Number of terms	$\bar{t} = 2.0$			$\bar{t} = 6.0$		
	$\widehat{T}(\frac{L_1}{2}, \frac{L_2}{2}, \frac{H}{2})$	$\widehat{T}(\frac{L_1}{2}, \frac{L_2}{2}, 0)$	$\widehat{T}(\frac{L_1}{2}, \frac{L_2}{2}, -\frac{H}{2})$	$\widehat{T}(\frac{L_1}{2}, \frac{L_2}{2}, \frac{H}{2})$	$\widehat{T}(\frac{L_1}{2}, \frac{L_2}{2}, 0)$	$\widehat{T}(\frac{L_1}{2}, \frac{L_2}{2}, -\frac{H}{2})$
5	1.960062	1.170248	1.004035	2.468455	1.656847	1.480494
10	1.994998	1.170763	1.015029	2.505207	1.660631	1.494150
15	1.997386	1.170742	1.014309	2.507529	1.660650	1.493503
20	1.997595	1.170739	1.014366	2.507733	1.660652	1.493561

$$\bar{\gamma} = \gamma t_r, \quad \bar{t} = \frac{t}{t_r}, \quad t_r = \frac{c_m \rho_m H^2}{\kappa_m}, \quad \bar{T} = \frac{T}{T^+}, \quad \bar{u}_i = \frac{u_i}{\alpha_m L_1 T^+}, \quad \bar{\sigma}_{ij} = \frac{\sigma_{ij}}{E_m \alpha_m T^+}. \tag{36}$$

Thus the reference length and the reference stress non-dimensionalizing displacements and stresses respectively equal the axial elongation of a free aluminum bar of length L_1 and the magnitude of the axial stress produced in this bar clamped at the edges caused by the temperature rise of T^+. t_r is the characteristic time of heat conduction through length H. For material properties listed in (33), $H = 50$ mm and $T^+ = 100$ K, these quantities respectively equal 0.585 mm, 63.8 MPa and 26 s.

The Mori–Tanaka homogenization scheme is used to find the effective material properties with the metal (Al) taken as the matrix phase and the ceramic (SiC) as the particulate phase. That is, $P_1 = P_m$ and $P_2 = P_c$, where P stands for either the volume fraction V or a material property. Fig. 3(a) depicts the time history of the prescribed temperature change on the mid-surface for $\gamma = 10$, 1.0 and 0.1 s^{-1}. It is clear that for $\gamma = 10$ s^{-1}, the temperature at the mid-surface rises rapidly to the steady state value, and the rise is more gradual for $\gamma = 0.1$ s^{-1}. For $L_1/H = 5$, Fig. 3(b)–(f) show the corresponding time evolution of the transverse displacement and stresses at different points in the plate. For $\gamma = 1$ and 10 s^{-1}, the transverse deflection at the center of the plate increases rapidly to its maximum value and then decreases slowly to its steady state value. However, for $\gamma = 0.1$ s^{-1}, the deflection is a monotonically increasing function of time. A similar trend is exhibited by the longitudinal stress $\bar{\sigma}_{11}$ at the center of the top surface of the plate. For $\gamma = 10$ s^{-1}, the longitudinal stress $\bar{\sigma}_{11}$ at $\bar{t} = 0.01$ is 7.9 times the steady state value. The magnitude of the shear stress $\bar{\sigma}_{12}$ at the left edge increases monotonically for all γ. The transverse shear stress $\bar{\sigma}_{13}(0, L_2/2, H/4, t)$ has a negative value initially and increases to a positive value when the steady state is reached. The transverse normal stress $\bar{\sigma}_{33}$ at the center of the plate is initially tensile and evolves to become compressive at steady state. The steady state temperature, displacement and stress fields match with the exact static thermoelasticity solution given by Vel and Batra (2002).

The through-the-thickness variation of the temperature and stresses is plotted in Fig. 4 for $\gamma = 10$ s^{-1}. The through-the-thickness variation of the longitudinal stress $\bar{\sigma}_{11}$, the transverse shear stress $\bar{\sigma}_{13}$ and the

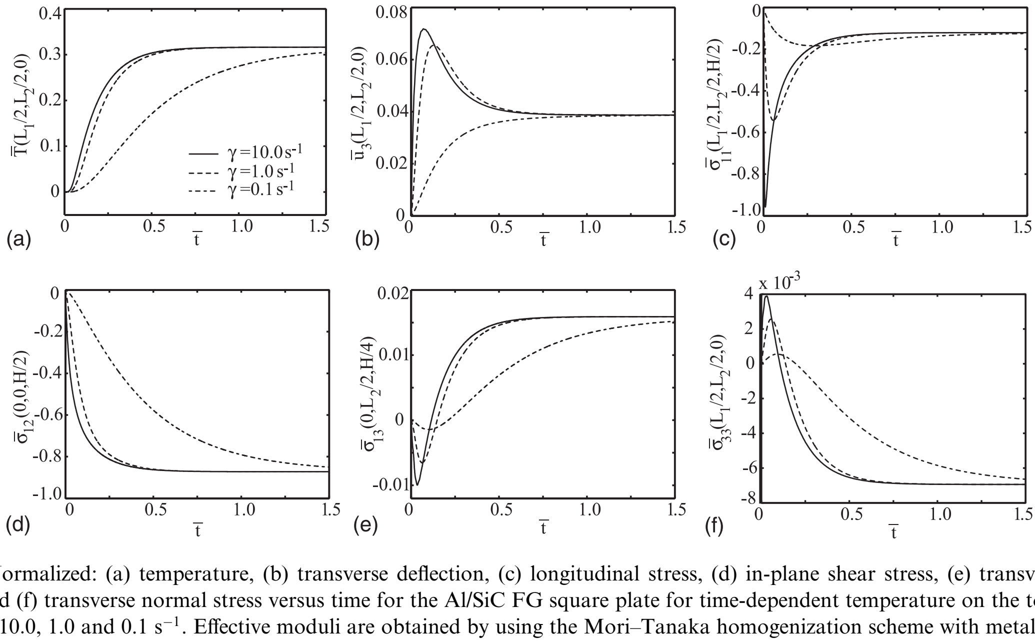

Fig. 3. Normalized: (a) temperature, (b) transverse deflection, (c) longitudinal stress, (d) in-plane shear stress, (e) transverse shear stress, and (f) transverse normal stress versus time for the Al/SiC FG square plate for time-dependent temperature on the top surface with $\gamma = 10.0$, 1.0 and 0.1 s^{-1}. Effective moduli are obtained by using the Mori–Tanaka homogenization scheme with metal as matrix and $V_c^- = 0$, $V_c^+ = 1$, $p = 2$, $L_1/H = 5$.

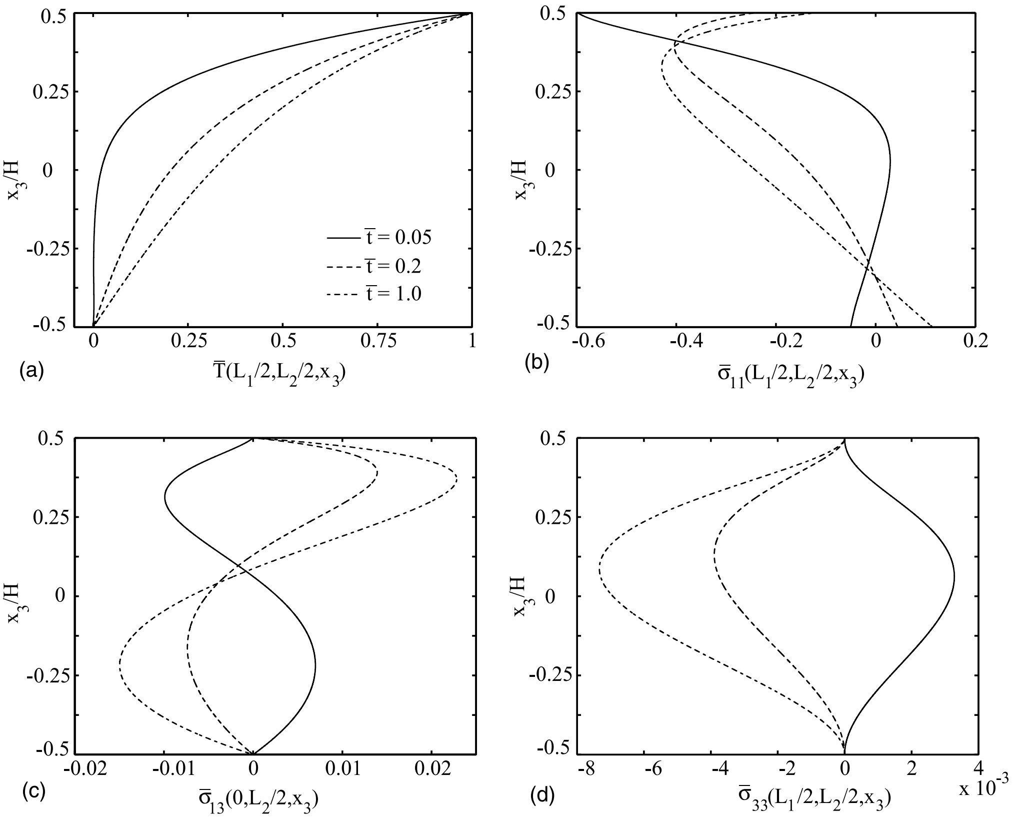

Fig. 4. Through-the-thickness variation of (a) temperature, (b) longitudinal stress, (c) transverse shear stress, and (d) transverse normal stress in the Al/SiC FG square plate for time-dependent temperature on the top surface with $\gamma = 10\ \mathrm{s}^{-1}$ at times $\bar{t} = 0.05$, 0.2 and 1.0. Effective moduli are obtained by using the Mori–Tanaka homogenization scheme with metal as matrix and $V_c^- = 0$, $V_c^+ = 1$, $p = 2$, $L_1/H = 5$.

transverse normal stress $\bar{\sigma}_{33}$ change significantly as a function of time. For example, at $\bar{t} = 0.05$ the magnitude of the longitudinal stress is maximum at a point on the top surface of the plate. However at $\bar{t} = 1.0$ the peak value of $|\bar{\sigma}_{11}|$ occurs at a point nearly one-sixth the height from the top surface. The magnitude of the axial stress at the center of the bottom surface always stays small even though the stress switches from compressive at $\bar{t} = 0.05$ to tensile at $\bar{t} = 1.0$. The transverse normal stress at a point on the midsurface changes from tensile at $\bar{t} = 0.05$ to compressive at $\bar{t} = 1.0$; its absolute value is nearly three order of magnitude smaller than that of the axial stress even though $H/L_1 = 0.2$. Similar comments apply to the transverse shear stress whose value is about one-tenth of that of the axial stress. The through-the-thickness variation of the longitudinal stress $\bar{\sigma}_{11}$ is non-linear since material properties and the temperature change vary through the thickness.

The time evolution of the temperature, transverse displacement and stresses for $\gamma = 1.0\ \mathrm{s}^{-1}$ and power-law exponent $p = 2$ are shown in Fig. 5 for various ceramic volume fractions V_c^+ on the top surface when $V_c^- = 0$. For $V_c^+ = 0$, results are for a homogeneous aluminum plate. The temperature and transverse deflection at the mid-surface decrease as the ceramic volume fraction on the top surface is increased; cf. Fig. 5a and b. Furthermore, the magnitude of the transient longitudinal thermal stress $\bar{\sigma}_{11}$ in an FG plate for $V_c^+ = 1.0$ is smaller than that in a homogeneous plate ($V_c^+ = 0$). The transverse shear stress

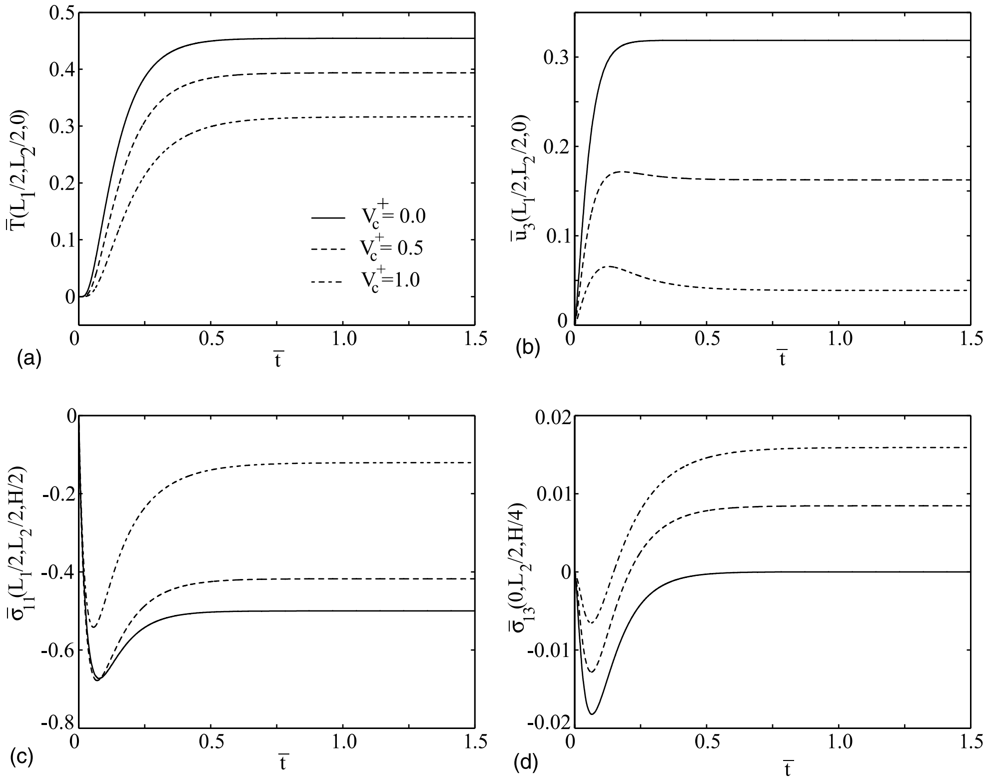

Fig. 5. Normalized: (a) temperature, (b) transverse deflection, (c) longitudinal stress, (d) transverse shear stress versus time for the Al/SiC FG square plate for volume fractions $V_c^+ = 0, 0.5$ and 1.0 and time-dependent temperature on the top surface with $\gamma = 1.0\ \mathrm{s}^{-1}$. Effective moduli are obtained by using the Mori–Tanaka homogenization scheme with metal as matrix and $V_c^- = 0$, $p = 2$, $L_1/H = 5$.

$\bar{\sigma}_{13}(0, L_2/2, H/4, t)$ is negative at all times for a homogeneous plate ($V_c^+ = 0$), whereas it evolves with time from a negative to a positive value for the two FG plates.

5.2. Time-dependent surface heat flux

The prescribed heat flux on the top surface increases from zero at $t = 0$ to a steady state value exponentially, and is given by

$$q_3(x_1, x_2, H/2, t) = q^+(\mathrm{e}^{-\gamma t} - 1)\sin(\pi x_1/L_1)\sin(\pi x_2/L_2), \tag{37}$$

and the heat flux on the bottom surface is zero, i.e., $q_3(x_1, x_2, -H/2, t) = 0$. The temperature, heat flux, displacements and stresses are non-dimensionalized as follows:

$$\widehat{T} = \frac{T\kappa_\mathrm{m}}{q^+H}, \quad \hat{q}_i = \frac{q_i}{q^+}, \quad \hat{u}_i = \frac{u_i\kappa_\mathrm{m}}{\alpha_\mathrm{m}L_1^2q^+}, \quad \hat{\sigma}_{ij} = \frac{\sigma_{ij}\kappa_\mathrm{m}}{E_\mathrm{m}\alpha_\mathrm{m}L_1q^+}. \tag{38}$$

Thus the reference value of the temperature equals the temperature difference across an aluminum bar of length H caused by the steady state heat flux of q^+ through it. The reference values of the displacement and the stress equal the elongation of a free bar of length L_1 and the magnitude of the axial stress developed in such a clamped bar with the steady state flux q^+ applied across the faces. For $q^+ = 10^6$ W/m^2, a value typical for laser heating, the reference temperature, displacement and stress equal respectively 214.6 K, 6.28 mm and 176 MPa.

The evolution of the temperature and the transverse displacement at the center of the plate, of the longitudinal stress at the center of the top surface, and of the transverse shear stress at the point $(0, L_2/2, H/4)$ on the left edge are depicted in Fig. 6 for $\gamma = 10$, 1 and 0.1 s^{-1} using the Mori–Tanaka homogenization scheme. The time history of the temperature rise at the center of the plate is essentially the same for $\gamma = 1$ and 10 s^{-1} but is a little lower for $\gamma = 0.1$ s^{-1}. For slow heating with $\gamma = 0.1$ s^{-1}, the magnitude of the longitudinal stress $\hat{\sigma}_{11}$ at the center of the top surface increases monotonically to the steady state value. However, if heat flux on the top surface increases rapidly, as would be the case for $\gamma = 10$ s^{-1}, the magnitude of the longitudinal stress $\hat{\sigma}_{11}(L_1/2, L_2/2, H/2)$ increases until $\bar{t} = 0.076$, decreases from $\bar{t} = 0.076$ to 0.237 and increases after that (Fig. 6c). Unlike for the problems of time-dependent surface temperatures, the transient thermal stresses for the time-dependent heat flux problems are less than their respective steady state values. It is because the magnitude of the temperature gradient in the thickness direction is smaller for the latter problems as compared to those of the former case. This is evidenced by the comparison of the through-the-thickness variations of the temperatures plotted in Figs. 4a and 7a for the two problems.

The through-the-thickness variation of the temperature and transverse displacement at the centerline of the plate, the longitudinal stress and of the transverse shear stress on the centerline of left edge for $\gamma = 10$ s^{-1} are plotted in Fig. 7. The ceramic volume fraction on the bottom and top surfaces are $V_c^- = 0.2$

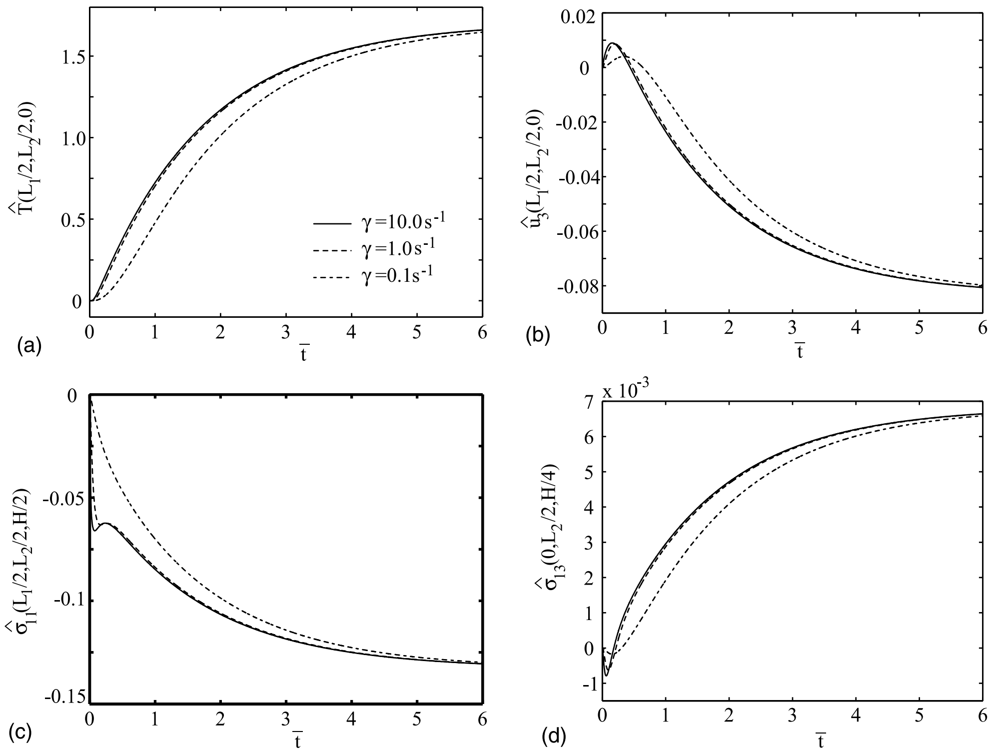

Fig. 6. Normalized: (a) temperature, (b) transverse deflection, (c) longitudinal stress, and (d) transverse shear stress versus time for the Al/SiC FG square plate for time-dependent heat flux on the top surface with $\gamma = 10.0$, 1.0 and 0.1 s^{-1}. Effective moduli are obtained by using the Mori–Tanaka homogenization scheme with metal as matrix and $V_c^- = 0$, $V_c^+ = 1$, $p = 2$, $L_1/H = 5$.

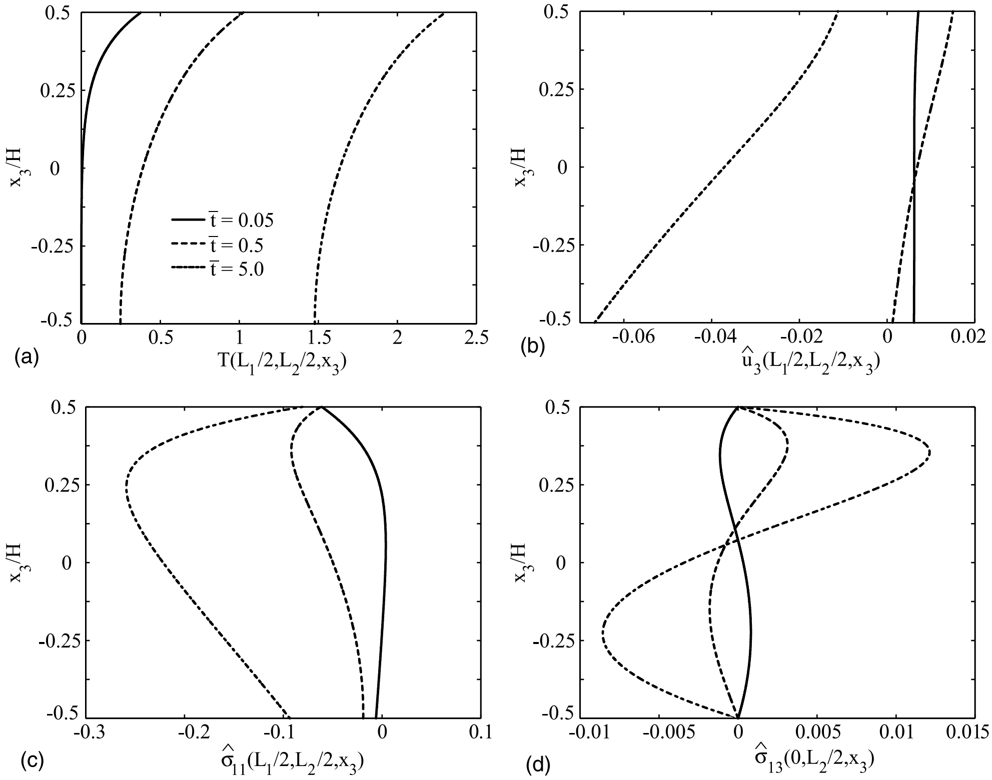

Fig. 7. Through-the-thickness variation of (a) temperature, (b) transverse displacement, (c) longitudinal stress and (d) transverse shear stress in the Al/SiC FG square plate for time-dependent heat flux on the top surface with $\gamma = 10\ \mathrm{s}^{-1}$ at times $\bar{t} = 0.05$, 0.5 and 5.0. Effective moduli are obtained by using the self-consistent homogenization scheme and $V_c^- = 0.2$, $V_c^+ = 0.8$, $p = 4$, $L_1/H = 5$.

and $V_c^+ = 0.8$, respectively, $p = 4$ and the effective properties are obtained by the self-consistent scheme. At time $\bar{t} = 5.0$, there is a significant difference in the transverse displacement of points on the top and bottom surfaces, indicating a considerable change in the thickness of the plate. The through-the-thickness variations of the longitudinal stress $\hat{\sigma}_{11}$ and the transverse shear stress $\hat{\sigma}_{13}$ are qualitatively and quantitatively different at different times (Fig. 7a and b); the peaks in their absolute values occur once the steady state has been reached.

5.3. Remarks on boundary conditions

A simply supported plate, loaded by compressive normal tractions on the top surface, is usually simulated in the laboratory by using sharp knife edges as supports. Assuming that the supports are rigid, points on the bottom surface of the four edges will be restrained from moving vertically and the edge surfaces will be traction free. Such boundary conditions can be easily simulated in numerical solutions of an initial-boundary-value problem as has been done by Batra and Geng (2001, 2002). However, due to singularities likely to occur at points of the plate contacting the sharp knife edges, it is difficult to satisfy such boundary conditions when solving the problem analytically. For the rectangular plate analyzed here, mechanical boundary conditions in (4) require that all points do not move in the plane of the edge surfaces and the normal component of the traction vector vanish. These boundary conditions can be obtained by bonding membranes with zero bending and infinite in-plane stiffness to the boundaries $x_1 = 0$, $x_1 = L_1$, $x_2 = 0$ and $x_2 = L_2$. Such support conditions are difficult to realize experimentally. However, the analytical solutions presented here are useful for validating plate theories and finite element formulations for FG plates. Three-dimensional analytical solutions presented by Srinivas and Rao (1970) and Pagano (1970) for laminated composite plates under boundary conditions (4) have been extensively used to assess the accuracy of classical and refined plate theories. Recently, Vel and Batra (1999, 2000, 2001) used the Stroh formalism to obtain three-dimensional analytical solutions for laminated plates subjected to arbitrary boundary conditions.

6. Conclusions

We have analysed 3D transient heat conduction problem for a rectangular simply supported FG plate with the uniform temperature prescribed at the edges and subjected to either time-dependent temperature or heat flux on the top and the bottom surfaces. The material properties are taken to be analytical functions of the thickness coordinate and are uniform in the other two directions. Transient stresses developed by the resulting temperature gradients have been evaluated for a simply supported FG plate. It is found that for the case of rapid time-dependent prescribed surface temperature, the transient longitudinal stress is nearly 8 times its steady state value. However, for the case of transient prescribed heat flux, the transient stresses are less than their respective steady state values. Furthermore, with the passage of time, longitudinal stresses at a point change from compressive to tensile and the transverse shear stresses change sign too. Qian and Batra (2003) have analyzed numerically transient thermomechanical deformations of an FG plate by using a higher-order shear and normal deformable plate theory of Batra and Vidoli (2002). They found that the consideration of inertia forces for problems involving transient thermal loads has a negligible effect on displacements and stresses induced in the plate.

Acknowledgements

RCB's work was partially supported by the ONR grant N00014-98-1-0300 to Virginia Polytechnic Institute and State University with Dr. Y.D.S. Rajapakse as the cognizant program manager.

References

Batra, R.C., Geng, T.S., 2002. Comparison of active constrained layer damping by using extension and shear mode actuators. Journal of Intelligent Materials and Structures 13, 349–368.

Batra, R.C., Geng, T.S., 2001. Enhancement of the dynamic buckling load for a plate by using piezoceramic actuators. Smart Materials and Structures 10, 925–933.

Batra, R.C., Vidoli, S., 2002. Higher order piezoelectric plate theory derived from a three-dimensional variational principle. AIAA Journal 40, 91–104.

Breval, E., Aghajanian, K., Luszcz, S.J., 1990. Microstructure and composition of alumina/aluminum composites made by the direct oxidation of aluminum. Journal of American Ceramic Society 73, 2610–2614.

Cheng, Z.Q., Batra, R.C., 2000. Three-dimensional thermoelastic deformations of a functionally graded elliptic plate. Composites: Part B 31, 97–106.

Fung, Y.C., Tong, P., 2001. Classical and Computational Solid Mechanics. World Scientific Publishing Co., Singapore.

Hashin, Z., 1968. Assessment of the self-consistent scheme approximation: conductivity of particulate composites. Journal of Composite Materials 2, 284–300.

Hatta, H., Taya, M., 1985. Effective thermal conductivity of a misoriented short fiber composite. Journal of Applied Physics 58, 2478–2486.

Hill, R., 1965. A self-consistent mechanics of composite materials. Journal of the Mechanics and Physics of Solids 13, 213–222.

Jin, Z.H., Batra, R.C., 1996a. Some basic fracture mechanics concepts in functionally graded materials. Journal of the Mechanics and Physics of Solids 44, 1221–1235.

Jin, Z.H., Batra, R.C., 1996b. Stress intensity relaxation at the tip of an edge crack in a functionally graded material subjected to a thermal shock. Journal of Thermal Stresses 19, 317–339.

Jin, Z.H., Batra, R.C., 1998. *R*-curve and strength behavior of a functionally gradient material. Material Science and Engineering A 242, 70–76.

Kim, K.S., Noda, N., 2001. Green's function approach to three-dimensional heat conduction equation of functionally graded materials. Journal of Thermal Stresses 24, 457–477.

Lambros, A., Narayanaswamy, A., Santare, M.H., Anlas, G., 1999. Manufacturing and testing of a functionally graded material. Journal of Engineering Materials and Technology 121, 488–493.

Mori, T., Tanaka, K., 1973. Average stress in matrix and average elastic energy of materials with misfitting inclusions. Acta Metallurgica 21, 571–574.

Ootao, Y., Tanigawa, Y., 1999. Three-dimensional transient thermal stresses of functionally graded rectangular plate due to partial heating. Journal of Thermal Stresses 22, 35–55.

Pagano, N.J., 1970. Exact solutions for rectangular bidirectional composites and sandwich plates. Journal of Composite Materials 4, 20–34.

Qian, L.F., Batra, R.C., 2003. Transient thermoelastic deformations of a thick functionally graded plate (submitted for publication).

Reiter, T., Dvorak, G.J., 1997. Micromechanical modelling of functionally graded materials. In: Bahei-El-Din (Ed.), IUTAM Symposium on Transformation Problems in Composite and Active Materials. Kluwer academic publishers, London, pp. 173–184.

Reiter, T., Dvorak, G.J., 1998. Micromechanical models for graded composite materials: II. Thermomechanical loading. Journal of the Mechanics and Physics of Solids 46, 1655–1673.

Reiter, T., Dvorak, G.J., Tvergaard, V., 1997. Micromechanical models for graded composite materials. Journal of the Mechanics and Physics of Solids 45, 1281–1302.

Rosen, B.W., Hashin, Z., 1970. Effective thermal expansion coefficients and specific heats of composite materials. International Journal of Engineering Science 8, 157–173.

Srinivas, S., Rao, A.K., 1970. Bending, vibration and buckling of simply supported thick orthotropic rectangular plates and laminates. International Journal of Solids and Structures 6, 1463–1481.

Tarn, J.Q., Wang, Y.M., 1995. Asymptotic thermoelastic analysis of anisotropic inhomogeneous and laminated plates. Journal of Thermal Stresses 18, 35–58.

Vel, S.S., Batra, R.C., 1999. Analytical solutions for rectangular thick laminated plates subjected to arbitrary boundary conditions. AIAA Journal 37, 1464–1473.

Vel, S.S., Batra, R.C., 2000. The generalized plane strain deformations of thick anisotropic composite laminated plates. International Journal of Solids and Structures 37, 715–733.

Vel, S.S., Batra, R.C., 2001. Generalized plane strain thermoelastic deformation of laminated anisotropic thick plates. International Journal of Solids and Structures 38, 1395–1414.

Vel, S.S., Batra, R.C., 2002. Exact solution for thermoelastic deformations of functionally graded thick rectangular plates. AIAA Journal 40, 1421–1433.

Vel, S.S., Batra, R.C., 2003a. Three-dimensional exact solution for the vibration of functionally graded rectangular plates. Journal of Sound and Vibrations (in press).

Vel, S.S., Batra, R.C., 2003b. Exact thermoelasticity solution for cylindrical bending deformations of functionally graded plates, Proceedings of the IUTAM Symposium on Dynamics of Advanced Materials and Smart Structures, Yonezawa, Japan, May 20–24, 2002, Watanabe, K., Ziegler, F. (Eds.), Kluwer academic publishers.

Yang, J., Shen, H.S., 2002. Vibration characteristics and transient response of shear-deformable functionally graded plates in thermal environment. Journal of Sound and Vibration 255, 579–602.